Journal of Macromolecular Science, Part B
Publication details, including instructions for authors and subscription information:
http://www.informaworld.com/smpp/title~content=t713375300

Morphological, Thermal, and Electrical Characterization of Syndiotactic Polypropylene/Multiwalled Carbon Nanotube Composites

E. Pollatos[a]; E. Logakis[b]; P. Chatzigeorgiou[a]; V. Peoglos[b]; I. Zuburtikudis[c]; M. Gjoka[d]; K. Viras[a]; P. Pissis[b]
[a] Laboratory of Physical Chemistry, Chemistry Department, National and Kapodistrian University of Athens, Panepistimiopolis, Athens, Greece [b] Department of Physics, School of Applied Mathematical and Physical Sciences, National Technical University of Athens, Zografou Campus, Athens, Greece [c] Department of Industrial Design Engineering, Technical Education Institute (T.E.I.) of Western Macedonia, Kozani, Greece [d] NCSR "Demokritos," Institute of Materials Science, Athens, Greece

Online publication date: 10 August 2010

To cite this Article Pollatos, E. , Logakis, E. , Chatzigeorgiou, P. , Peoglos, V. , Zuburtikudis, I. , Gjoka, M. , Viras, K. and Pissis, P.(2010) 'Morphological, Thermal, and Electrical Characterization of Syndiotactic Polypropylene/Multiwalled Carbon Nanotube Composites', Journal of Macromolecular Science, Part B, 49: 5, 1044 — 1056
To link to this Article: DOI: 10.1080/00222341003609708
URL: http://dx.doi.org/10.1080/00222341003609708

Journal of Macromolecular Science®, Part B: Physics, 49:1044–1056, 2010

ISSN: 0022-2348 print / 1525-609X online
DOI: 10.1080/00222341003609708

Morphological, Thermal, and Electrical Characterization of Syndiotactic Polypropylene/Multiwalled Carbon Nanotube Composites

E. POLLATOS,[1] E. LOGAKIS,[2] P. CHATZIGEORGIOU,[1] V. PEOGLOS,[2] I. ZUBURTIKUDIS,[3] M. GJOKA,[4] K. VIRAS,[1] AND P. PISSIS[2]

[1]Laboratory of Physical Chemistry, Chemistry Department, National and Kapodistrian University of Athens, Panepistimiopolis, Athens, Greece
[2]Department of Physics, School of Applied Mathematical and Physical Sciences, National Technical University of Athens, Zografou Campus, Athens, Greece
[3]Department of Industrial Design Engineering, Technical Education Institute (T.E.I.) of Western Macedonia, Kozani, Greece
[4]NCSR "Demokritos," Institute of Materials Science, Athens, Greece

In this work, syndiotactic polypropylene/multiwalled carbon nanotubes (MWCNT) nanocomposites, in various concentrations, were produced using melt mixing. The influence of the addition of MWCNT on the morphology, crystalline form, and the thermal and electrical properties of the polymer matrix was studied. To that aim, scanning electron microscopy, Raman spectroscopy, X-ray diffraction, differential scanning calorimetry, and dielectric relaxation spectroscopy were employed. Significant alterations of both the crystallization behavior and the thermal properties of the matrix were found on addition of the carbon nanotubes: conversion of the disordered crystalline form I to the ordered one, increase of the crystallization temperature and the degree of crystallinity, and decrease of the glass transition temperature and the heat capacity jump. Finally, the electrical percolation threshold was found between 2.5–3.0 wt.% MWCNT. For comparison purposes, the results of the system studied here are also correlated with the findings from a previous work on the isotactic polypropylene/MWCNT system.

Keywords carbon nanotubes, electrical properties, morphology, nanocomposites, syndiotactic polypropylene, thermal properties

Introduction

Among a wide variety of commercially important polymers, polypropylene currently has the highest growth rate. The most common commercial form is isotactic polypropylene (iPP), while syndiotactic polypropylene (sPP) is not so widely used. Its lower melting

Received 15 September 2009; accepted 29 October 2009.
Address correspondence to Emmanuel Logakis, Department of Physics, School of Applied Mathematical and Physical Sciences, National Technical University of Athens, Zografou Campus, Athens, Greece. E-mail: logmanos@central.ntua.gr

point, lower degree of crystallinity, and relatively slow crystallization rate are some of the reasons for that. On the other hand, because of its relatively low degree of crystallinity and small crystal size, sPP has a higher clarity and is more ductile, at room temperature, with a greater impact strength when compared with iPP.[1,2] However, the necessity of improving the sPP properties is crucial in order to widen the range of its commercial applications.

Polymer properties are remarkably improved by the addition of carbon nanotubes (CNT) when compared with virgin polymers. Since their discovery by Iijima in 1991,[3] CNT have been used in many technological applications. Their very appealing physical and mechanical properties, such as high elastic modulus, as well as remarkable thermal and electrical conductivity made them ideal inclusions by industry in high-performance polymers.[4] Especially, their high electrical conductivity, in combination with their very high aspect ratio (length to diameter ratio >1000), enables the preparation of conducting composites at very low filler contents, suitable for numerous applications such as electromagnetic interference shielding, electrostatic dissipation, gas sensors, etc.[5]

Several methods have been developed for the incorporation of CNT in a polymer matrix.[4–6] The melt mixing technique was used in our study, taking into account the simplicity and the low cost of the method. Additionally, this technique is free of solvents, the required equipment is already available in the plastic industry and permits recycling of the preconsumer scrap.

Despite the large number of available articles referred to iPP/CNT systems,[7–12] the influence of the addition of CNT on the physical properties of sPP matrix is not so well studied. In this article, the morphological and thermal properties of sPP/multiwalled carbon nanotubes (MWCNT) nanocomposites are investigated by employing various techniques (scanning electron microscopy, X-ray diffraction, Raman spectroscopy, differential scanning calorimetry). Special attention is paid to the changes induced by the presence of CNT on the crystallization behavior and the thermal transitions of the sPP matrix. The transition from the insulating to the conducting phase at a certain amount of CNT (the so-called percolation threshold) is also investigated by employing dielectric relaxation spectroscopy. The results are correlated with those of our previous work in iPP/MWCNT composites[12] and interesting relationships are found.

Experimental Part

Materials

sPP, in pellet form, was obtained from Sigma-Aldrich (melt flow index: 4.5 g/10 min, M_n: 54,000, M_w: 127,000). MWCNT were purchased from Nanothinx S.A. The nanotubes were produced by the chemical vapor deposition method (purity $\geq$95%, average diameter 10–30 nm, average length $\approx$10 μm).

The nanocomposites were prepared by melt mixing. The mixing was done in a corotating, conical, twin-screw microextruder/compounder (ThermoHaake MiniLab^{TM}) at 180°C for over 30 min and at a mixing speed of 200 r min^{-1} in N_2 atmosphere. Slabs with a thickness of 0.5 mm were prepared by compression molding of the mixed composites using a custom hydraulic press at 15 MPa for 5 min initially and at 30 MPa for additional 5 min, while the temperature was kept at 170°C. Then, the temperature was lowered from 170°C to 30°C under ambient conditions. The final obtained concentration of MWCNT in the prepared nanocomposites varied from 0.5 to 5.0 wt.%.

Experimental Techniques

The morphology of sPP/MWCNT composites was observed using scanning electron microscopy (SEM) (FE Inspect SEM, Philips) operating with an acceleration voltage of 20 kV. SEM samples were cryofractured in liquid nitrogen and their fractured surface was sputtered with gold before taking the images to prevent charging.

Differential scanning calorimetry (DSC) measurements were carried out in the temperature range from −70°C to 180°C using a PerkinElmer Pyris 6 apparatus. A cooling rate of 10 K min^{-1} and a heating rate of 10 K min^{-1} were used. The weight of the samples varied from 4 to 6 mg. It is noted that both sPP and its composite samples containing various MWCNT amounts were first heated from room temperature (30°C) to 180°C and held there for 5 min (first heating), in order to remove any previous thermal history. All measurements were carried out in nitrogen atmosphere.

X-ray diffraction (XRD) patterns were taken on a Siemens D500 diffractometer, using CuKα radiation of a wavelength of $\lambda = 0.154$ nm. Measurements were performed over the range 2θ from 5° to 55°, at steps of 0.04° and counting time of 5 s.

Raman spectra were recorded on a Perkin–Elmer GX Fourier Transform spectrometer. A diode-pumped Nd:YAG laser exciting at 1064 nm was used. The scattered radiation was collected at an angle of 180° to the incident beam. Spectra were recorded at a laser power of 30 mW at the sample with a resolution of 4 cm^{-1} and an interval of 2 cm^{-1}. In order to obtain a good signal to noise ratio, 1000 scans were coadded for the spectra. The Raman spectra were taken in the spectral region 100–3500 cm^{-1}.

The electrical and dielectric properties of the prepared materials were studied by employing dielectric relaxation spectroscopy (DRS). In this technique, the sample is placed between the plates of a capacitor, an alternate voltage is applied, and the response of the system is studied. By measuring the complex impedance ($Z^* = Z' - iZ''$) of the circuit, the complex permittivity ($\varepsilon^* = \varepsilon' - i\varepsilon''$) can be obtained from the following equation:[13]

$$\varepsilon*(\omega) = \frac{1}{i\omega Z^*(\omega) C_0}, \tag{1}$$

where ω is the angular frequency ($\omega = 2\pi f$) of the applied electric field and C_0 the equivalent capacitance of the free space. The complex permittivity is the most common formalism to describe the electrical and dielectric relaxation phenomena. The frequency-dependent ac conductivity (real part, σ') is then obtained from the following equation:[13]

$$\sigma'(\omega) = \varepsilon_0 \omega \varepsilon''(\omega), \tag{2}$$

where $\varepsilon_0 = 8.85 \times 10^{-12}$ F m^{-1} is the permittivity of free space.

DRS measurements were carried out at room temperature in the frequency range of 10^{-2}–10^6 Hz by means of a Novocontrol Alpha analyzer. Further details about the experimental apparatus can be found in.[14]

Results and Discussion

Morphological Characterization

Figure 1 shows typical SEM images, in two magnification levels for the nanocomposite containing 5.0 wt.% MWCNT [Figs. 1(b) and 1(c)] and a neat sPP film for comparison purposes [Fig. 1(a)]. The micrographs show that MWCNT, which are observed as white spots, are uniformly dispersed in the polymer matrix even for the highest loading of

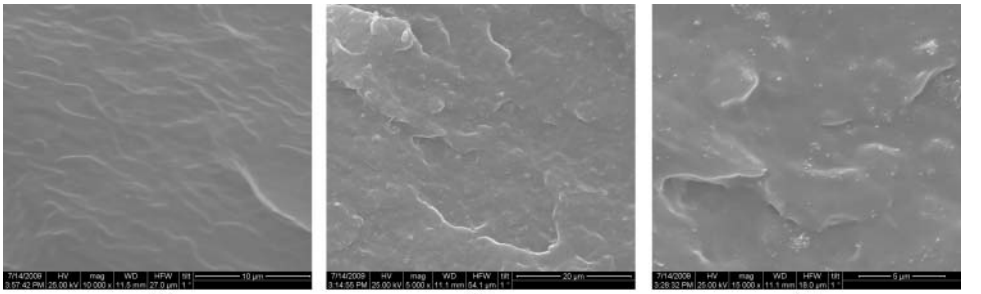

Figure 1. SEM micrographs for (a) the pure sPP matrix and (b and c) the nanocomposite containing 5 wt.% MWCNT, in two magnification levels.

5.0 wt.%. Some small agglomerates that can be detected are also uniformly dispersed in the sPP matrix (see the larger-scale images). The homogenous dispersion of the fillers is a crucial parameter affecting all the physical properties (thermal, electrical, mechanical, etc.) of the nanocomposites.

Crystallization and Thermal Transitions

sPP can form four different crystalline and one mesomorphic forms. The crystallite forms I and II exhibit helical conformation, whereas the form III adopts the *trans*-planar conformation and can be obtained upon quenching or stretching ([15] and references therein). Form III can be transformed to form IV upon exposure to organic solvents.[15] The main interest here is to look for any effects of the MWCNT addition on the crystallization behavior and on the thermal transitions of the sPP matrix. To that aim, XRD and DSC measurements were employed.

Figure 2 shows XRD patterns for the pure sPP matrix and its nanocomposites. All the examined samples contain the characteristic diffraction peaks of the most usual form I of sPP at $2\theta = 12.3^\circ$, 15.9°, 20.5°, and 24.7, which correspond to the (200), (010), (210) and (400) reflections planes, respectively.[16] Furthermore, the peak at $2\theta = 15.9^\circ$ is not symmetric, showing a shoulder at $2\theta = 17^\circ$, typical of the *trans*-planar mesophase. It has

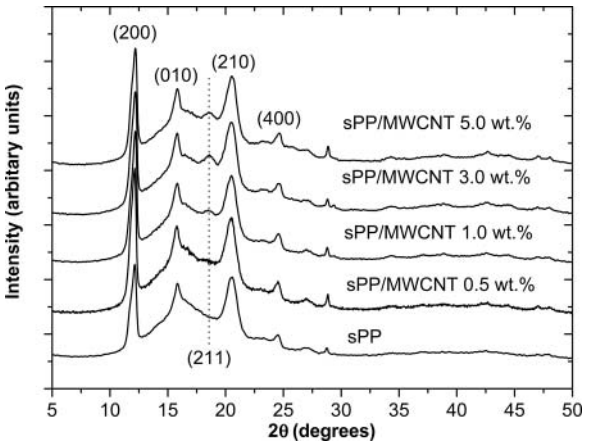

Figure 2. XRD patterns for the pure sPP and the nanocomposites, as indicated on the plot.

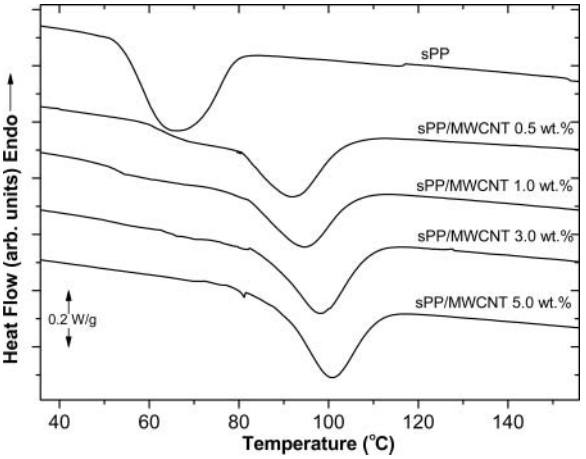

Figure 3. Crystallization thermograms for pure sPP and the nanocomposites, as indicated on the plot (cooling rate: 10 K min^{-1}).

been shown that the *trans*-planar mesophase can be formed by quenching the sample from the melt to 0°C and holding it at that temperature for a long time.[17] This phase is stable up to 80°C, whereas at 90°C, it is almost completely transformed into the more stable form I.[17] However, our results show that this mesophase can be also formed by cooling down the molten sample from 170°C to 30°C at a low rate (without any quenching procedure). Another interesting point is that, while in the pure sPP the diffraction peak at $2\theta = 18.9°$, which corresponds to the (211) plane of form I, is absent, in the nanocomposites, this peak is present and its intensity increases as the amount of MWCNT increases. The absence of this diffraction peak in the pure sPP indicates the existence of the disordered modification of the form I.[18,19] On the contrary, the addition of the nanotubes promotes the formation of the most stable form I [the (211) peak being clearly present]. It is noted that further analysis of the XRD spectra to obtain further information about the crystal size was not examined as the complex XRD patterns introduce high errors during the analysis. Only the (200) diffraction peak was possible to be accurately analyzed, with the results showing no significant changes to the crystal size due to MWCNT addition (the width varied between 128 and 136Å).

Figure 3 shows DSC thermograms during cooling for the pure sPP matrix and sPP/MWCNT nanocomposites (cooling rate: 10 K min^{-1}). The observed exothermic peaks are attributed to the crystallization of the sPP matrix. The addition of the MWCNT causes a large initial increase of the crystallization temperature (T_c) (from 65.4°C to 91.6°C on addition of 0.5 wt.%) and then a gradual shift to higher temperatures (up to 100.6°C for the highest amount of MWCNT), indicating the action of CNT as nucleating agents (Table 1). This behavior has been reported previously in the literature for iPP[20,21] and other semicrystalline matrixes, such as polyamide,[22–25] polystyrene,[26] and so on. It is noted that the nucleation ability of CNT usually leads to an increase in crystallization temperature by about 10°C upon addition to the polymeric matrices (see [24] and references therein). Here this increase is significantly higher, denoting a stronger nucleating action of CNT in the crystallization of sPP compared with iPP and other polymer matrices. It is also interesting to note that, in contrast to DSC findings in iPP/MWCNT and PA6/MWCNT

Table 1

Melting temperature (T_m), heat of fusion (ΔH_m), heat of fusion normalized to the polymer mass ($\Delta H_m{}^*$), degree of crystallinity (X_c), and crystallization temperature ($T_{c,1}$) for the pure sPP matrix and sPP/MWCNT nanocomposites. The errors in temperatures are estimated to $\pm$ 0.5°C, whereas errors in enthalpies and in degree of crystallinity are in the order of 5%

	Melting				
Sample	T_m(°C)	ΔH_m (J g^{-1})	ΔH_m *(J g^{-1})	X_c (%)	Crystallization T_c(°C)
sPP	112.4 and 126.4	35.5	35.5	19.4	65.4
sPP/0.5 wt.% MWCNT	123.5	36.7	36.9	20.2	91.6
sPP/1.0 wt.% MWCNT	124.2	40.4	40.8	22.3	94.3
sPP/3.0 wt.% MWCNT	125.6	41.4	42.7	23.3	97.9
sPP/5.0 wt.% MWCNT	125.8	37.0	38.9	21.3	100.6

systems, where a second crystallization peak appeared on the addition of CNT (owing to trans-crystallinity),[12,25] this behavior is absent here.

In Fig. 4, melting thermograms (second heating) are presented for the sPP and its nanocomposites at a heating rate of 10 K min^{-1}. For the pure sPP, two main melting peaks are observed, located at 112.4°C and 126.4°C. The lower temperature melting peak corresponds to the melting of the primary crystallites formed, while the higher temperature melting peak is a result of the melting of the crystallites recrystallized during the heating scan.[15,27] On the contrary, in the case of the nanocomposites only the high temperature melting peak appears. This result suggests that the presence of the CNT promotes the formation of better formed crystals, in agreement with the previously mentioned XRD findings. Nevertheless, a shoulder in the high temperature side of the peak appears in

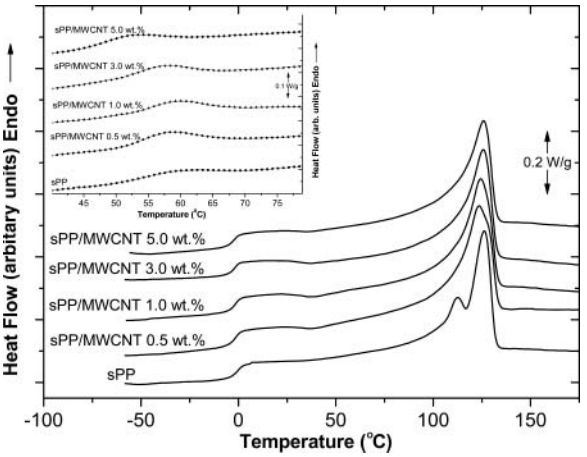

Figure 4. Melting thermograms for pure sPP and the nanocomposites, as indicated on the plot (heating rate: 10 K min^{-1}). In the inset, the first heating scan is presented (heating rate: 10 K min^{-1}), focused in the temperature region where the mesophase is observed.

the nanocomposites (it is more prominent for the samples containing 0.5 and 1.0 wt.% MWCNT), indicating a broader crystallite size distribution on addition of the nanotubes.

The degree of crystallinity was calculated from the melting thermograms by the following equation:

$$X_c\ (\%) = \frac{\Delta H_m}{(1-\varphi)\Delta H_0} \times 100, \tag{3}$$

where ΔH_m is the measured heat of fusion, ΔH_0 is the heat of fusion for 100% crystalline sPP and φ is the weight fraction of MWCNT in the nanocomposites. ΔH_0 was taken equal to 183 J g^{-1}.[16] The results listed in Table 1 show a slight increase of X_c by the addition of the nanotubes. It is mentioned that these findings were consistent with the results obtained by XRD. The latter are not shown here since it is more secure to base the calculations on DSC measurements, as the analysis of XRD spectra, because of their complexity in the case of polypropylene, contains several sources of error. Nevertheless, both techniques showed the same tendency: increase of X_c as the amount of MWCNT increases. It is noted that the highest loaded sample, containing 5.0 wt.%, deviates from that behavior: although more external nucleating sites are present, the high amount of MWCNT probably restricts the motion (diffusion) of the polymeric chains during the crystallization process.

In the inset to Fig. 4 the thermograms of the first heating scan are also presented for the sPP and its nanocomposites at a heating rate of 10 K min^{-1}. In all the samples a small endotherm is observed, between 50°C and 70°C, because of the melting of the *trans*-planar mesophase. The existence of this mesophase is in agreement with the aforementioned XRD findings. This mesophase no longer exists during the second heating (thermograms in Fig. 4), as it was already transformed to form I during the first heating and did not reform during cooling.

Finally, in the temperature region of −10°C to 10°C, a step in heat flow appears (Fig. 4) indicating the glass transition of the amorphous sPP phase. The glass transition temperature (T_g) (calculated as the midpoint of the extrapolated heat capacities before and after the glass transition), the glass transition width ($\Delta T_g = T_{g,\,onset} - T_{g,\,end}$, where $T_{g,onset}$ and $T_{g,\,end}$ are defined as the intersections between the extrapolated tangents before and after the glass transition, respectively, and the extrapolated tangent at the inflection point), the heat capacity jump at the glass transition (ΔC_p) and the normalized heat capacity to the mass of the amorphous polymer ($\Delta C_p^* = \Delta C_p/[(1-\varphi)(1-X_c)]$) are listed in Table 2. The

Table 2

Glass transition temperature (T_g), glass transition width (ΔT_g), heat capacity jump at the glass transition (ΔC_p), and normalized heat capacity (ΔC_p^*). The errors in temperatures are estimated to ± 0.5°C, whereas errors in heat capacities are in the order of 5%

	Glass transition			
Sample	T_g(°C)	ΔT_g(°C)	ΔC_p(J g^{-1} K^{-1})	ΔC_p^*(J g^{-1} K^{-1})
Spp	−0.7	8.2	0.34	0.42
sPP/0.5 wt.% MWCNT	−1.9	6.9	0.31	0.39
sPP/1.0 wt.% MWCNT	−2.0	6.2	0.32	0.41
sPP/3.0 wt.% MWCNT	−2.4	6.2	0.28	0.37
sPP/5.0 wt.% MWCNT	−2.6	5.8	0.25	0.34

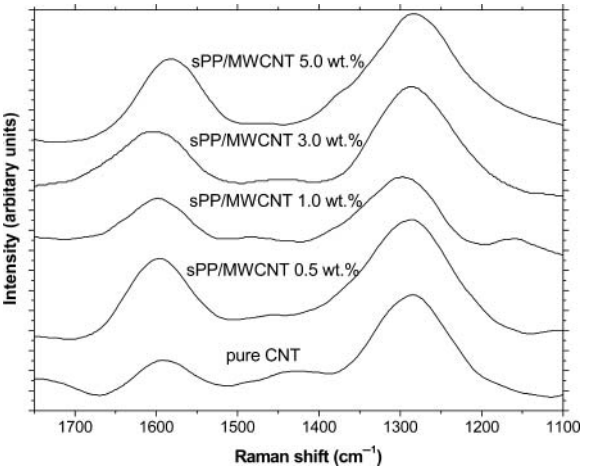

Figure 5. High-frequency Raman spectra of MWCNT and sPP/MWCNT composites.

results show a slight decrease in the glass transition of the pure sPP matrix on addition of MWCNT. Similar behavior has been already mentioned in other semicrystalline polymer nanocomposites containing CNT[25] and is explained by the free volume concept.[25,28] The introduction of the CNT, by preventing the packing of the polymer chains, increases the free volume of the system. In that way, the cooperative motion of the polymer chains (glass transition) can be observed at a lower temperature. It is noted that an increase or even no change of T_g has also been reported in various polymeric matrices on addition of nanosized particles.[29]

Additionally, the normalized heat capacity (ΔC_p^*) decreases in the nanocomposites, indicating that a smaller fraction of the amorphous phase contributes to the glass transition. This result can be interpreted in terms of a two-layer model in which one part of the polymer is immobilized near the inclusions (an interfacial layer with partially or completely suppressed mobility), because of strong polymer–filler interactions,[30,31] and only the rest participates normally to the glass transition.[25] Contrarily, in iPP/MWCNT composites, no significant change in ΔC_p^* was observed. To that point it is interesting to take into account the existence of a *trans*-crystallinity in the iPP/MWCNT system, as it was revealed by DSC measurements.[12] It seems that this crystalline layer, which is developed around the CNT walls, prohibits the interactions between the fillers and the amorphous phase, and consequently all the amorphous phase participates in the glass transition.

Raman Spectroscopy

Raman characterization was applied to underline the effects of MWCNT on the polymer matrix composites. Raman spectra of sPP/MWCNT composites typically show intense peaks in the spectral ranges of 1100–1750 cm^{-1} and 135–200 cm^{-1}. Figure 5 shows the high-frequency Raman spectra of MWCNT and the various nanocomposites (0.5, 1.0, 3.0 and 5.0 wt.%). The Raman bands of the MWCNT are clearly identified, but the sPP ones do not appear because of their low intensity. The spectra exhibit characteristic MWCNT peaks at 1285 cm^{-1} and 1595 cm^{-1}. The first, assigned to the D band, derives from disordered graphite structures, while the second one, assigned to the G band, is associated

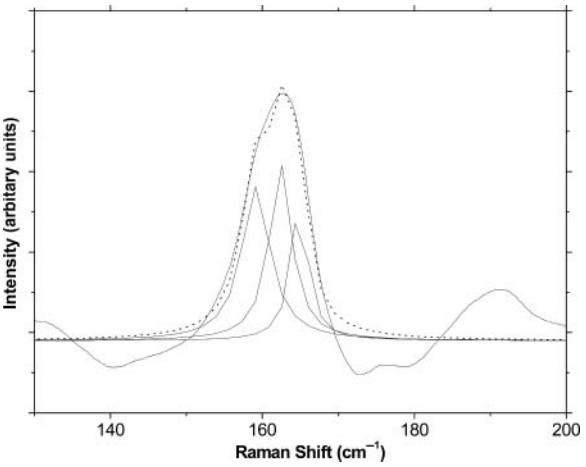

Figure 6. Low-frequency Raman spectrum of sPP/0.5 wt.% MWCNT composite.

with tangential C&bond;C bond stretching motions that originate from the E_{2g2} mode at 1580 cm^{-1} in graphite.[32]

By increasing the nanotube concentration in the polymer matrix, the G band is upshifted from 1587 cm^{-1} (pure CNT) to 1604 cm^{-1} (3.0 wt.%), as shown in Fig. 5. The shifting of the band to higher frequencies can be attributed to the disentanglement of nanotubes and subsequent dispersion in the sPP matrix as a consequence of polymer penetration into the nanotubes bundles during the melt mixing process. The latter is expected to contribute significantly to the influence of the crystallization, because of the increase of the formation of nucleating agents that favor the crystallization process, as was already discussed. Only the sample with the highest CNT content (5.0 wt.%) deviates from this behavior, and the G band is downshifted to 1585 cm^{-1} (Fig. 5). This is in agreement with the DSC results where a decrease of crystallinity is observed. Similar upshifting of the G band has been reported for SWCNT/ iPP[20] and reinforced epoxy resins,[33] as well as for polyethylene matrix.[34]

Using the peak height Raman intensities of the G and D bands in the equation $I_G/(I_G+I_D) \times 100\%$, the degree of graphitization of CNT was found to be 45%.[35]

The low-energy bands in Raman spectra are attributed to a radial breathing mode (RBM) where all C atoms are subject to an in-phase radial displacement, associated with a symmetric movement of all carbon atoms in the radial direction. The frequency of the RBM mode is proportional to the inverse of the tube inner diameter (1/d) according to the equation: $\omega_{RBM} = 223.5/d + 12.5$, where ω_{RBM} is given in centimeters inverse and d in nanometers.[32]

A prominent RBM band at about 163 cm^{-1} was recorded in the spectra of MWCNT and in sPP/MWCNT composites. Band component analysis (Fig. 6) gave three main bands at 159, 162, and 164 cm^{-1}, which correspond to nanotubes with inner diameters 1.52, 1.49, and 1.47 nm, respectively.

Electrical Properties

DRS was employed to study the electrical properties of the prepared nanocomposites. Figure 7 shows ac conductivity (σ') at room temperature as a function of frequency (f), for

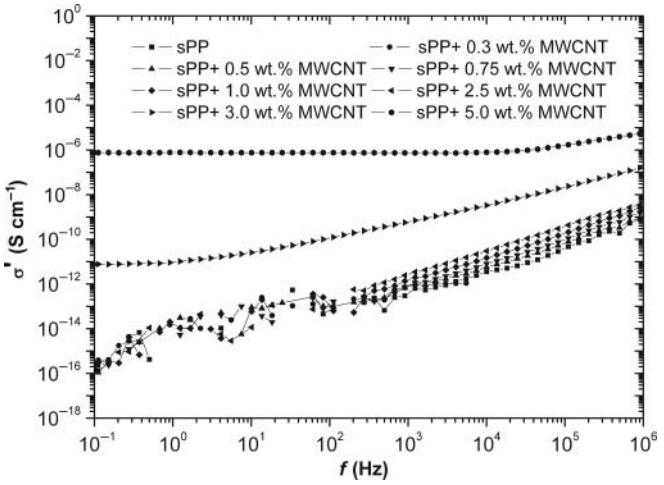

Figure 7. Conductivity (σ') vs. frequency (f) at room temperature for the samples indicated on the plot.

the pure sPP and the compositions indicated on the plot. For pure sPP and the nanocomposites containing 0.3, 0.5, 0.75, 1.0, and 2.5 wt.% MWCNT, ac conductivity increases approximately linearly with the frequency in a logarithmic scale, exhibiting a typical capacitor behavior. Contrarily, for the nanocomposites containing 3.0 and 5.0 wt.% MWCNT, a dc plateau, where conductivity is independent of frequency, appears below the critical frequency f_c, indicating the transition from the insulating to the conducting phase [the so-called percolation threshold (p_c)]. Detailed description for the above mentioned behavior (called universal dynamic response)[36,37] is given in [14].

The percolation threshold, located between 2.5–3.0 wt.% MWCNT, is in the same order with previous mentioned ones in sPP/MWCNT and iPP/MWCNT systems.[11,19] Significant lower values have been also reported in iPP/MWCNT systems by optimizing both the melt flow index of the polypropylene used and the mixing conditions.[12] The melt flow index of the matrix, and consequently the viscosity of the melt, is one of the most crucial parameters in order to obtain polymer nanocomposites with low p_c values. The low viscosity, on the one hand, facilitates the dispersion of the fillers and, on the other hand, prevents the breakage of the nanotubes because of the high shear forces that are induced during the mixing.

Conclusions

Nanocomposites of sPP containing multiwalled CNT were prepared using melt mixing. SEM measurements revealed a homogeneous dispersion of MWCNT. DSC and XRD measurements showed significant changes in the thermal transitions and crystallization of the sPP matrix. Both pure sPP matrix and its nanocomposites were crystallized in the most usual form I, showing also the *trans*-planar mesophase. The addition of CNT caused the conversion from the disordered form I to the most stable modification of form I. This result is particularly significant and should be further followed in the future by studying the influence of this conversion on the mechanical properties of the nanocomposites. Furthermore, the action of MWCNT as external nucleating sites was verified by the sifting of the

crystallization temperature to higher values. This sifting is more pronounced in the case of sPP, indicating a stronger nucleating action of the nanotubes, comparing with previous mentioned results in iPP/MWCNT composites. As concerns the glass transition region, a slight decrease of T_g was recorded. Additionally, the heat capacity jump decreased upon MWCNT incorporation. This behavior can be understood by adopting a two-layer model, where one part of the polymer near the interface is partially or completely immobilized and does not participate in the cooperative motion of the polymeric chains, giving rise to the observed ΔC_p^* reduction. It is interesting to note that the above mentioned description is not consistent with the findings in iPP/MWCNT composites, where ΔC_p^* remained unaffected by the presence of the nanotubes, denoting weaker polymer–filler interactions. Finally, the electrical properties of the nanocomposites were studied by employing DRS. The percolation threshold was found between 2.5 and 3.0 wt.% MWCNT and satisfactory levels of conductivity, as concerns potential applications (such as electromagnetic interference shielding and electrostatic dissipation), were obtained only at the highest loaded sample (5.0 wt.% MWCNT).

Acknowledgments

This work has been funded by the project PENED 2003. The project is cofinanced 75% of public expenditure through EC—European Social Fund, 25% of public expenditure through Ministry of Development—General Secretariat of Research and Technology and through private sector, under measure 8.3 of OPERATIONAL PROGRAMME "COMPETITIVENESS" in the 3rd Community Support Programme.

References

1. Loos, J.; Bonnet, M.; Petermann, J. Morphologies and mechanical properties of syndiotactic polypropylene (sPP)/polyethylene (PE) blends. Polymer **2000**, *41*, 351.
2. Arranz-Andrés, J.; Guevara, J.L.; Velilla, T.; Quijada, R.; Benavente, R.; Pérez, E.; Cerrada, M.L. Syndiotactic polypropylene and its copolymers with alpha-olefins. Effect of composition and length of comonomer. Polymer **2005**, *46*, 12287.
3. Iijima, S. Helical microtubules of graphitic carbon. Nature **1991**, *354*, 56.
4. Breuer, O.; Sundararaj, U. Big returns from small fibers: A review of polymer/carbon nanotube composites. Polym. Compos. **2004**, *25*, 630.
5. Moniruzzaman, M.; Winey, K.I. Polymer nanocomposites containing carbon nanotubes. Macromolecules **2006**, *39*, 5194.
6. Grossiord, N.; Loos, J.; Regev, O.; Koning, C.E. Toolbox for dispersing carbon nanotubes into polymers to get conductive nanocomposites. Chem. Mater. **2006**, *18*, 1089.
7. Sandler, J.; Broza, G.; Nolte, M.; Schulte, K.; Lam, Y.M.; Shaffer, M.S.P. Crystallization of carbon nanotube and nanofiber polypropylene composites. J. Macromol. Sci. Phys. **2003**, *B42*, 479.
8. López Manchado, M.A.; Valentini, L.; Biagiotti, J.; Kenny, J.M. Thermal and mechanical properties of single-walled carbon nanotubes—polypropylene composites prepared by melt processing. Carbon **2005**, *43*, 1499.
9. Abdolhosein, F.; Morteza, G.A.; Seyfolah, S. Thermal and structural behaviors of polypropylene nanocomposites reinforced with single-walled carbon nanotubes by melt processing method. J. Macromol. Sci. Phys. **2008**, *B48*, 196.
10. Peneva, Y.; Valcheva, M.; Minkova, L.; Mičušik, M.; Omastová, M. Nonisothermal crystallization kinetics and microhardness of PP/CNT composites. J. Macromol. Sci. Phys. **2008**, *B47*, 1197.
11. Mičušik, M.; Omastová, M.; Krupa, I.; Prokeš, J.; Pissis, P.; Logakis, E.; Pandis, Ch.; Pötschke, P.; Pionteck, J. A comparative study on the electrical and mechanical behaviour of multi-walled

carbon nanotube composites prepared by diluting a masterbatch with various types of polypropylenes. J. Appl. Polym. Sci. **2009**, *113*, 2536.
12. Logakis, E.; Pollatos, E.; Pandis, Ch.; Peoglos, V.; Zoubourtikoudis, I.; Delidis, C.G.; Vatalis, A.; Gjoka, M.; Syskakis, E.; Viras, K.; Pissis, P. Structure-property relationships in isotactic polypropylene/multi-walled carbon nanotubes nanocomposites. Compos. Sci. Technol. **2010**, *70*, 328.
13. Kremer, F.; Schoenhals, A. *Broadband Dielectric Spectroscopy*. Springer: Germany, **2002**, p. 37, 81.
14. Logakis, E.; Pandis, Ch.; Peoglos, V.; Pissis, P.; Pionteck, J.; Pötschke, P.; Mičušík, M.; Omastová, M. Electrical/dielectric properties and conduction mechanism in melt processed polyamide/multi-walled carbon nanotubes composites. Polymer **2009**, *50*, 5103.
15. Gregoriou, G.V.; Kandilioti, G.; Bollas, T.S. Chain conformational transformations in syndiotactic polypropylene/layered silicate nanocomposites during mechanical elongation and thermal treatment. Polymer **2005**, *46*, 11340.
16. Zhang, X.; Li, R.; Kong, L.; Wang, D. Stress-induced structure transition of syndiotactic polypropylene via melt spinning. Polymer **2008**, *49*, 1350.
17. Vittoria, V.; Guadagno, L.; Comotti, A.; Simonutti, R.; Auriemma, F.; De Rosa, C. Mesomorphic form of syndiotactic polypropylene. Macromolecules **2000**, *33*, 6200.
18. Sarno, M.; Gorassi, G.; Sannino, D.; Sorrentino, A.; Ciambelli, P.; Vittoria, V. Polymorphism and thermal behaviour of syndiotactic poly(propylene)/carbon nanotube composites. Macromol. Rapid Commun. **2004**, *25*, 1963.
19. Gorassi, G.; Romeo, V.; Sannino, D.; Sarno, M.; Ciambelli, P.; Vittoria, V.; De Vivo, B.; Tucci, V. Carbon nanotube induced structural and physical property transitions of syndiotactic polypropylene. Nanotechnology **2007**, *18*, 275703.
20. Valentini, L.; Biagiotti, J.; Kenny, J.M.; Santucci, S. Effects of single-walled carbon nanaotubes on the crystallization behavior of polypropylene. J. Appl. Polym. Sci. **2003**, *87*, 708.
21. Assouline, E.; Lustiger, A.; Barber, A.H.; Cooper, C.A.; Klein, E.; Wachtel, E.; Wagner, H.D. Nucleation ability of multiwall carbon nanotubes in polypropylene composites. J. Polym. Sci. Part B Polym. Phys. **2003**, *41*, 520.
22. Li, J.; Fang, Z.; Tong, L.; Gu, A.; Liu, F. Polymorphism of nylon-6 in multiwalled carbon nanotubes/nylon-6 composites. J. Polym. Sci. Part B Polym. Phys. **2006**, *44*, 1499.
23. Liu, T.; Phang, I.Y.; Shen, L.; Chow, S.Y.; Zhang, W.D. Morphology and mechanical properties of multiwalled carbon nanotubes reinforced nylon-6 composites. Macromolecules **2004**, *37*, 7214.
24. Phang, I.Y.; Ma, J.; Shen, L.; Liu, T.; Zhang, W.D. Crystallization and melting behavior of multi-walled carbon nanotube-reinforced nylon-6 composites. Polym. Int. **2006**, *55*, 71.
25. Logakis, E.; Pandis, Ch.; Peoglos, V.; Pissis, P.; Stergiou, Ch.; Pionteck, J.; Pötschke, P.; Mičušik, M.; Omastová, M. Structure—property relationships in polyamide6/multi-walled carbon nanotubes nanocomposites. J. Polym. Sci. Part B Polym. Phys. **2009**, *47*, 764.
26. Hiong, X.; Gao, Y.; Li, H.M. Non-isothermal crystallization kinetics of syndiotactic polystyrene–polystyrene functionalized SWNTs nanocomposites. eXPRESS Polym. Lett. **2007**, *1*, 416.
27. Supaphol, P. Crystallization and melting behavior in syndiotactic polypropylene: Origin of multiple melting phenomenon. J. Appl. Polym. Sci. **2001**, *82*, 1083.
28. Goertzen, W.K.; Kessler, M.R. Dynamic mechanical analysis of fumed silica/cyanate ester nanocomposites. Composites Part A **2008**, *39*, 761.
29. Paul, D.R.; Robeson, L.M. Polymer nanotechnology: Nanocomposites. Polymer **2008**, *49*, 3187.
30. Bershtein, V.A.; Egorova, L.M.; Yakushev, P.N.; Pissis, P.; Sysel, P.; Brozova, L. Molecular dynamics in nanostructure polyimide-silica hybrid materials and their thermal stability. J. Polym. Sci. Part B Polym. Phys. **2002**, *40*, 1056.
31. Gomez Tejedor, J.A.; Rodriguez Hernandez, C.J.; Gomez Ribelles, J.L.; Monleon Pradas, M.J. Dynamic mechanical relaxation of poly(2-hydroxyethyl acrylate)-silica nanocomposites obtained by the sol-gel method. J. Macromol. Sci. Phys. **2007**, *B46*, 43.

32. Dresselhaus, M.S.; Dresselhaus, G.; Saito, R.; Jorio, A. Raman spectroscopy of carbon nanotubes. Phys. Rep. **2005**, *49*, 47.
33. Puglia, D.; Valentini, L.; Kenny, J.M. Analysis of the cure reaction of carbon nanotubes/epoxy resin composites through thermal analysis and Raman spectroscopy. J. Appl. Polym. Sci. **2003**, *88*, 452.
34. McNally, T.; Potschke, P.; Halley, P.; Murphy, M.; Martin, D.; Bell, S.E.J.; Brennan, G.P.; Bein, D.; Lemoine, P.; Quinn, J.P. Polyethylene multiwalled carbon nanotube composites. Polymer **2005**, *46*, 8222.
35. Gojny, F.H.; Wichmann, M.H.G.; Fielder, B.; Kinloch, I.A.; Bauhofer, W.; Windle, A.H.; Schulte, K. Evaluation and identification of electrical and thermal conduction mechanisms in carbon nanotube/epoxy composites. Polymer **2006**, *47*, 2036.
36. Jonscher, A.K. The 'universal' dielectric response. Nature **1977**, *267*, 673.
37. Dyre, J.C.; Schroder, T.B. Universality of ac conduction in disordered solids. Rev. Mod. Phys. **2000**, *72*, 873.